Properties of the long-term oscillations in the middle atmosphere based on observations from TIMED/SABER

Yiyao Zhang [1], Shudao Zhou [1,*] ,Hanqing Shi [1],Zheng Sheng [1,2,],Weilai Shi [1],Huadong Du[1], and Zhiqiang Fan[1]**

[1]   College of Meteorology and Oceanology, PLA University of Science and Technology, Nanjing, China

[2]   Collaborative Innovation Center on Forecast and Evaluation of Meteorological Disasters,

   Nanjing University of Information Science & Technology, Nanjing, China

*   Correspondence: sq20112@163.com; Tel.: +86-15261821348
** Correspondence: 19994035@sina.com; Tel.: +86-13915955593

Abstract: The properties of the annual, semiannual and triennial oscillations (AO, SAO and TO) in the middle atmosphere have been investigated using the TIMED/SABER temperature data. The lomb-Scargle and wavelet spectra were used to determine the dominant oscillations in the background temperature field. The AO is prominent at the mid-latitudes. The AO amplitudes present an asymmetry between the two Hemispheres, being larger in the mesosphere than in the stratosphere. The SAO dominates the tropical regions, with three amplitude maxima at altitudes of 45, 75, and 85 km. The SAOs in the upper mesosphere (75 km) are out of phase with those in the mesopause (85 km) in the tropical regions, which can generate an enhancement of 11 K at each equinox, contributing to the lower mesospheric inversion layer. The TO is significant in the tropical region, with amplitude being maximum at 35, 45 and 85 km. Result shows that there may be potential interaction by the TO with SAO at 85km at the equator. The relation between ENSO and the TO has also been discussed Result is that the ENSO signal may modulate the amplitude of the TO, mainly in the lower stratosphere, and the real origin of the TO may possibly lie in the wave-mean-flow interaction.

Keywords: AO; SAO; TO; amplitude; phase

1. Introduction

The amount of observational data on atmospheric temperature is increasing, owing to marked improvements in the methods of measurement. However, observations of the middle atmosphere lag behind significantly because of a lack of global observations and measurement methods. Generally, the middle atmosphere refers to altitudes between 20–100 km, mainly including the stratosphere, the mesosphere, and the lower thermosphere. There is now a pressing need to know the precise temperature structure of the middle atmosphere, especially in the mesosphere and lower thermosphere (MLT). This is important for the investigation of dynamic processes and global climate changes. Furthermore, with more accurate temperature observations, the accuracy of numerical models can be verified and improved.

Several ground-based techniques have been used to investigate mesospheric temperature climatology. Lidar observations provide temperature profiles from 30–~85 km by collecting Rayleigh backscattering signals, but mostly only at night [1]. Meteoric radar uses underdense meteor decay times collectively to make reasonable estimates of the temperature in the mesopause [2]. There are also other ground-based observations concerning mesospheric temperature, such as sounding

46   rockets [3] and weather balloons [4]. However, the data collected by such ground-based technologies
47   are inadequate for the analysis of the global temperature structure because they cover only a limited
48   region and observations over oceans are scarce. Fortunately, satellite observations offer an effective
49   way to remedy this situation.
50   Various satellite measurements have been used to research the global temperature structure.
51   The Solar Mesosphere Explorer (SME) satellite provided near-global temperature observations for
52   40–92 km with relatively high vertical resolution (4 km) [5]. The Halogen Occultation Experiment
53   (HALOE) on the Upper Atmosphere Research Satellite (UARS) measured temperatures between
54   sunrise and sunset [6]. Remsberg et al. [7] derived the global structure of the temperature amplitude
55   and phase of both the annual and semiannual oscillations (AO and SAO), based on 9.5 years of
56   HALOE data at altitudes of ~32–80 km. More recently, GPS radio occultation (RO) has become a
57   powerful tool in atmospheric temperature sounding, with excellent vertical resolution and precision
58   in all weather conditions; however, its horizontal resolution is relatively low [8].
59   Observations from most satellites are generally limited by their vertical range and poor
60   sampling in local time. None could provide comprehensive observations until the launch of the
61   TIMED (Thermosphere, Ionosphere, Mesosphere Energetics and Dynamics) satellite in December
62   2001. The Sounding of the Atmosphere using Broadband Emission Radiometry (SABER) instrument
63   on TIMED has been making observations since late January 2002. Huang et al. [9] and Xu et al. [10]
64   have used the SABER temperature data of versions 1.04 (2002–2004) and 1.06 (2002–2006),
65   respectively, to analyze the global structure of zonal mean temperature variations of AO, SAO, and
66   quasi-biennial oscillations (QBO).
67   The period of time covered by the data has now increased, with the SABER 2.0 data set being
68   more accurate than the previous versions. In addition, no previous work has focus on the
69   morphologies and origins of the TO.
70   In this paper, the SABER 2.0 temperature data are used to analyze the AO, SAO and TO in the
71   middle atmosphere. The organization of the rest of this paper is as follows. A detailed introduction
72   to the data set and the analysis method is provided in section 2. In section 3, Lomb–Scargle spectral
73   analysis is used to identify the significant variations in the middle atmosphere. In section 4, the
74   global structure and the inter-annual variations of AO and SAO are analyzed. Section 5 shows the
75   relationship between the SAO and the mesospheric inversion layer (MIL). In section 6, the
76   morphologies, possible interaction with AO and SAO and the origins of TO are discussed, and
77   section 7 gives the conclusions of the paper.
78

2. Data and method

80   a. TIMED/SABER temperature data

81   The TIMED satellite is in a circular orbit at 625 km with an inclination of 74.1°. The latitude
82   coverage of TIMED is from 52°N to 83°S or 52°S to 83°N, which means that the satellite can always
83   access the latitude range from 52°S to 52°N. As the orbit of TIMED precesses slowly, there is a
84   procession of ~12 min in local time between two successive days. Over ~60 days, the satellite samples
85   a full 24 h of local time.
86   The SABER detector on the TIMED satellite is a limb observation instrument, with kinetic
87   temperature being derived from CO_2 infrared limb radiance at tangent altitudes of 15–120 km. In the
88   mesosphere, the effects of non-local thermodynamic equilibrium (NLTE) must be considered in the
89   retrieval scheme [11-12].
90   In this paper, we use the SABER temperature product of Custom Level 2A, Version 2.0 from
91   January 2002 to February 2015. SABER temperature data are accurate at altitudes of 20–60 km [13].
92   The NLTE algorithm has been improved substantially in the upper mesosphere and lower

93   thermosphere (UMLT) in versions after 1.06 [14], describing well the characteristics of long-term
94   variations and tides.
95   Atmospheric variations can be decomposed into several components, including mean waves,
96   tides, and planetary waves [10,15]. In order to eliminate tides and planetary waves so as to obtain
97   more accurate estimates of the zonal mean temperature, a 60-day sliding window with a 1-day step
98   is used to deal with the raw data. In practice, this means incorporating successive 60-day
99   observations into a 60-day data set, used as day 31 of the 60 days. A bin of 1 km×5° is then applied to
100 calculate the zonal mean for the central latitudes and altitudes. Since 52° pole-ward observations
101 only exist on alternate yaw cycles, the central latitudes of this paper are extended from 50°S to 50°N,
102 with a resolution of 5°. The vertical profiles are spaced from 20–120 km, with an interval of 1 km.
103 Note that the incompletely sampled satellite data cannot fully separate the mean temperature and
104 tides, so aliasing from the tides to zonal mean temperature remains a general problem, as discussed
105 by Oberheide et al. [16]. Thus, care must be taken when analyzing the mesospheric SAO, which has
106 certain properties in common with the migrating diurnal tide [17].
107 b. Analysis methods
108   Lomb–Scargle spectral analysis [18] and wavelet analysis [19] can be used to identify the typical
109 oscillations in the middle atmosphere. The main components of the oscillations can be fitted to the
110 following approximation:

$$T(t) = A_0 + A_1 \cos(\omega_0(t - t_{ao})) + A_2 \cos(2\omega_0(t - t_{sao})) + T_{rend}t + \delta_t \qquad (1)$$

111 Equation (1) suggests that the mean temperature field can be decomposed into five parts. For a given
112 altitude and latitude, T(t) is the zonal mean temperature that varies with time, and A_0 is the average
113 climatic state. $\omega_0 = 2\pi / 365$ represents the circular frequency of the AO, while the circular frequency
114 of the SAO is 2ω_0 . A_1 and A_2 are the amplitudes of the AO and SAO, and t_{ao} and t_{sao} are the phases.
115 T_{rend} is the long-term trend in the mean temperature, and δ_t is the residual error between the fitting
116 results and the observations. The nonlinear least squares fitting method is applied to determine the
117 parameters of the equation. Using this method, the global structures of the phase and amplitude of
118 AO and SAO, and the inter-annual variations are derived.
119

(**a**)
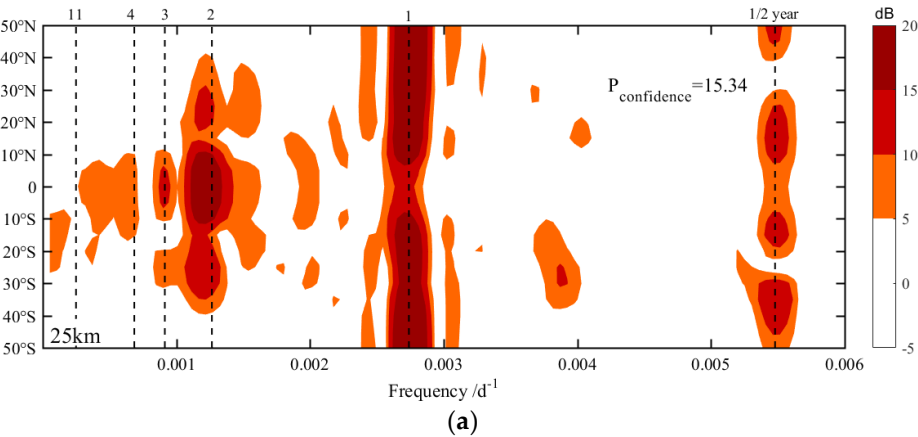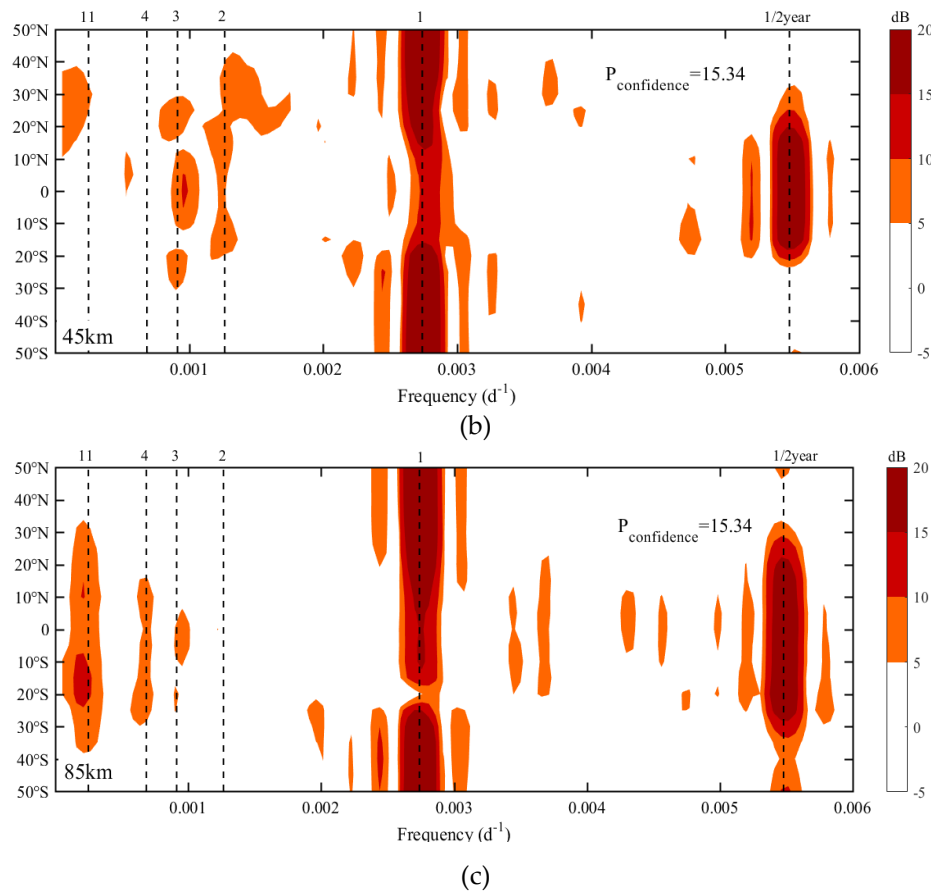
Figure 1. Lomb–Scargle spectral analysis of zonal mean temperature.

(a) for 25 km, (b) for 45 km, (c) for 85 km.

3. Lomb–Scargle spectral analysis

With the method of Lomb–Scargle spectral analysis, several components are identified in the middle atmosphere. Apart from AO, SAO, and QBO, longer oscillations also exist in the middle atmosphere (e.g. triennial oscillation and the 11- year oscillation). In this section, three typical altitudes are chosen: 25, 45, and 85 km. Figure 1 shows the Lomb–Scargle spectral analysis of the zonal mean temperatures. The shaded areas denote a confidence level of 99%. The power value is defined as $P_{dB} = 10\log10(P/P_{confidence})$, where $P_{confidence}=15.34$ is the corresponding power value obtained for a confidence level of 99%, and P is the power value of the Lomb–Scargle spectral analysis. Figure 1a shows that the AO and QBO are prominent at 25 km. Note that the periodicity of the QBO in the stratosphere is not fixed and is >2 years on average. Hence, the QBO has a period of 26 months in our analysis, as found by Huang et al. (2006)[9]. It is also shown in Figure 1a that the QBO is the main oscillation between 20°S and 20°N in the lower stratosphere, corresponding to the result given by Huang et al. [9,20].

Figures 1b and 1c show the structure of variations in the upper stratosphere and the mesopause, respectively. The similar features are that the SAO dominates the equatorial regions while the AO is prominent at mid-latitudes. An apparent difference is that the stronger 11-year oscillations exist at 85 km, with a peak around 20°S, although they are weaker than the AOs and SAOs presented. The 11-year oscillations are seen in the mesosphere and lower thermosphere (MLT) and become stronger

141   in the UMLT (figures not shown). Clemesha et al. [21] and Huang et al. [22] indicate that the 11-year

142   oscillations seen in the MLT are highly correlated with the varying ultraviolet flux of the 11-year

143   solar cycle.

144   It is obvious in Figure 1 that the AO and SAO are the most prominent zonal mean oscillations in

145   the middle atmosphere, Their morphologies are in agreement with previous studies (e.g. [7,10]). In

146   addition, the 3-year oscillation signal, which is significant as well as the QBO and SAO, especially at

147   around 45 km over the equatorial region, has attracted our attention. This triennial oscillation (TO)

148   has been discovered in previous researches (e.g. [23]), hovever, no further work has focus on its

149   morphologies and origins. The principal objective of this paper is characterization of the AO ,SAO

150   and TO.

151

(**a**)   (**b**)
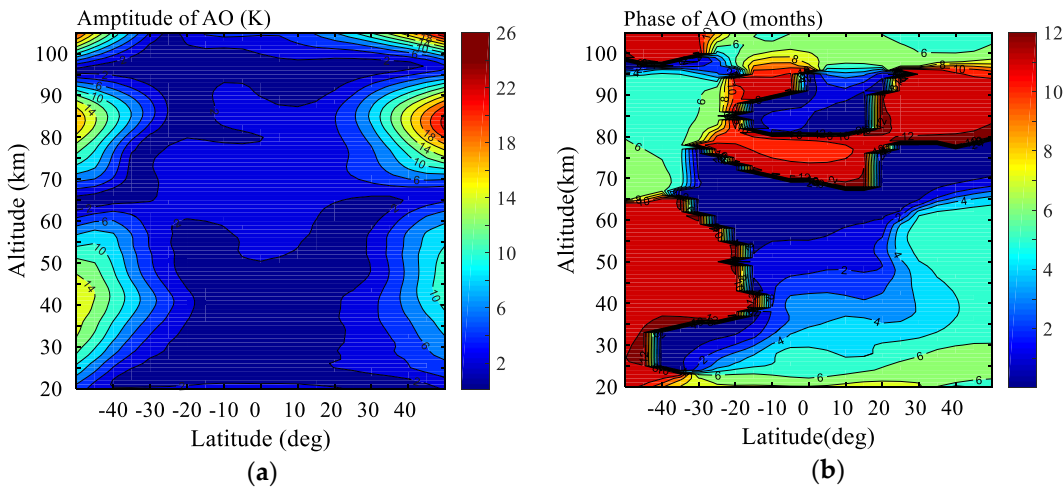
152   Figure 2. Distribution of (a) amplitude (K) and (b) phase (months) of AO.

153   Contour intervals are 2 K and 1 month.

154
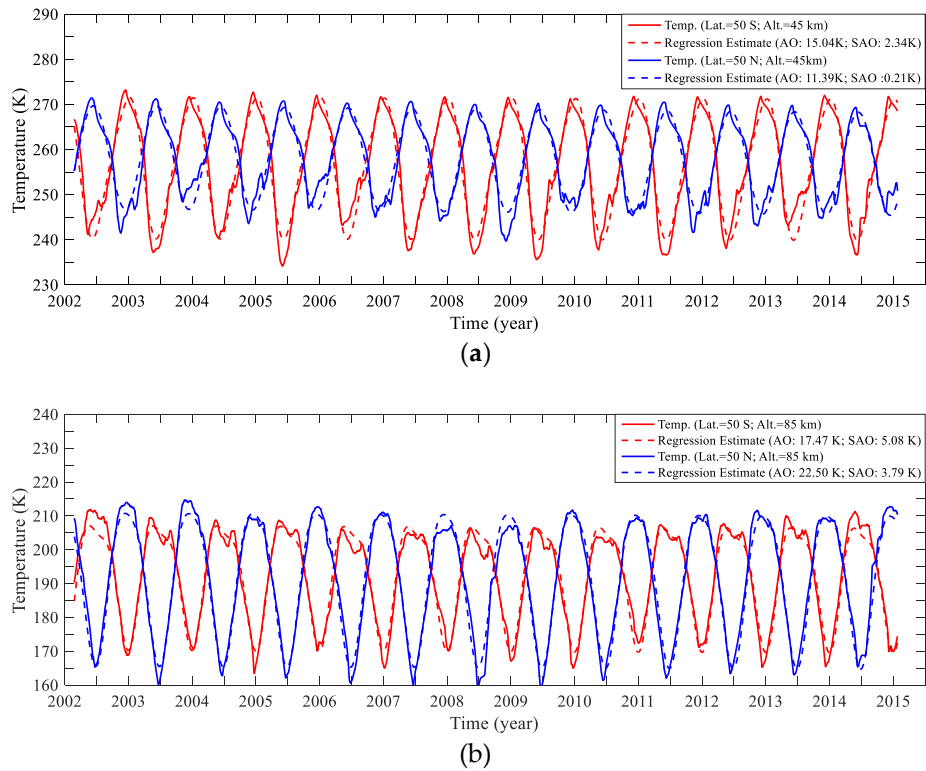
155   Figure 3. Time series of zonal mean temperature. (a): red for 50°S 45 km, blue for 50°N 45 km; (b):
156   red for 50°N 85 km, blue for 50°N 45 km.

157

(g)   (h)
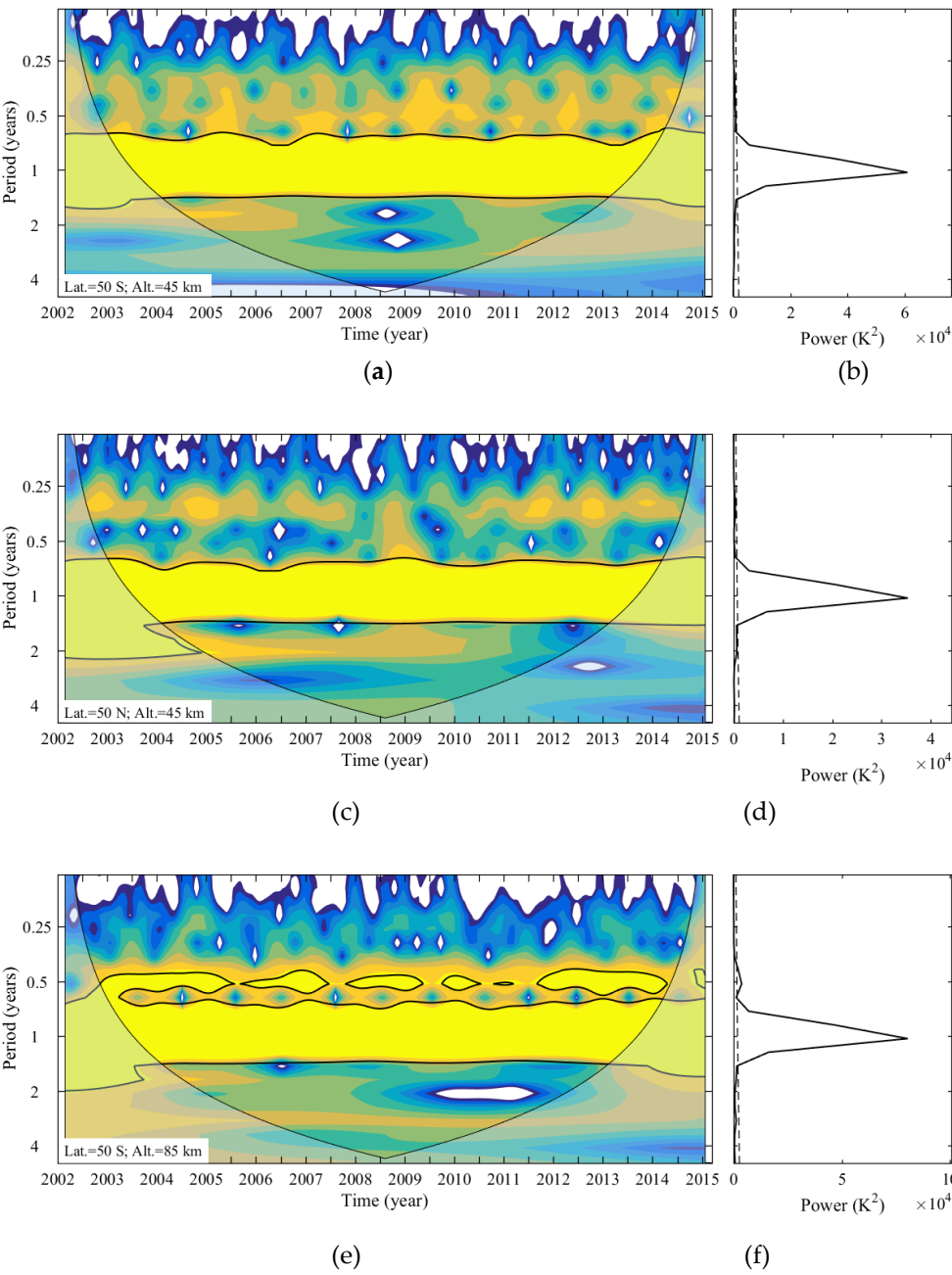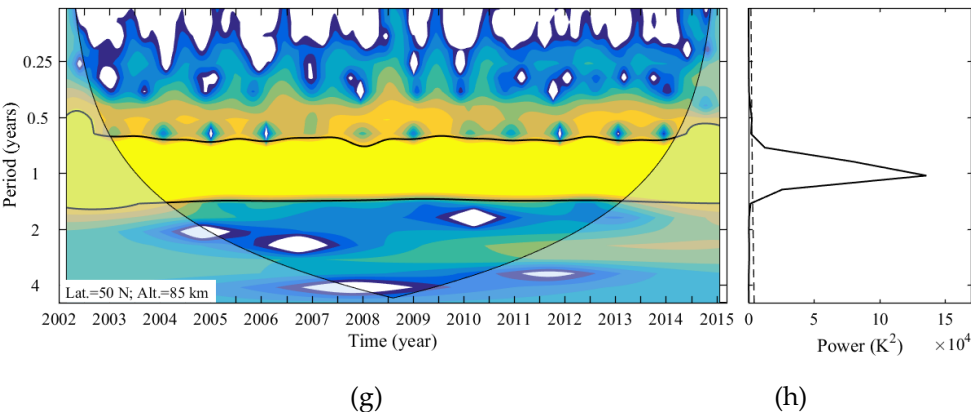
Figure 4. The wavelet power spectrum and the global power spectrum of time series at different altitudes and latitudes. (a), (b): Lat.=50°S, Alt.=45 km; (c), (d): Lat.=50°N, Alt.=45 km; (e), (f):Lat.=50°S, Alt.=85 km; (g), (h):Lat.=50°N, Alt.=85 km. Note that the Morlet wavelet normalized by standard deviation is used here. The thick-contour-enclosed regions are the places where there is greater than 95% confidence for a red-noise process with a lag-1 coefficient of 0.72. Transparent regions indicate the 'cone of influence,' where the edge effects become important, which means that anything in this region is dubious. The global wavelet spectrum is on the right side of the wavelet power spectrum. The dashed line is the 95% confidence level for the global wavelet spectrum.

(a)   (b)
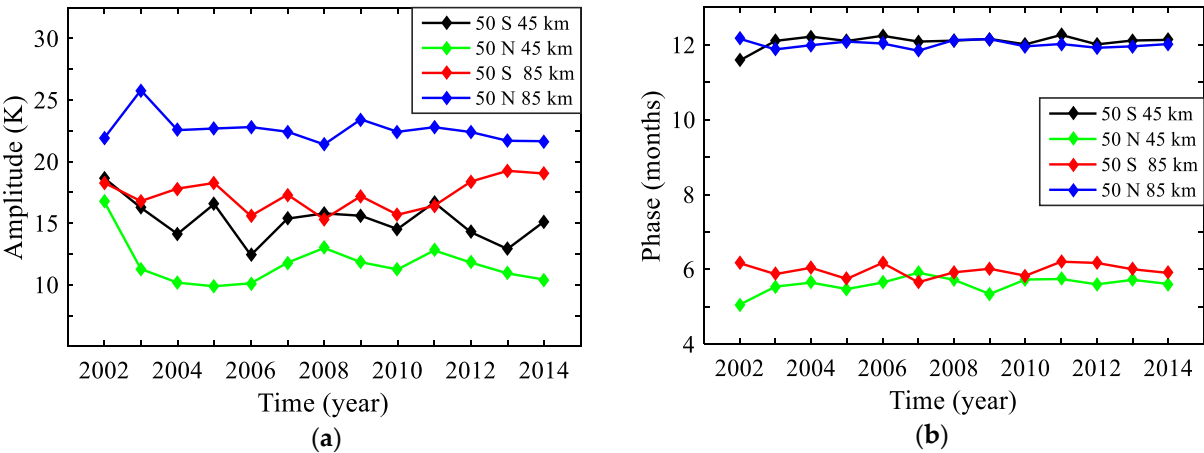
Figure 5. Variations of (a) amplitudes and (b) phases of the AO for 50°S 45 km, 50°N 45 km, 50°S 85 km, and 50°N 85 km.

4. Analysis of the main zonal mean temperature variations

4.1. Annual oscillation (AO)

The global pattern of the amplitude and phase of the AO are given in Figure 2 for altitudes of 20–105 km. As shown in Figure 2a, the AO dominates the regions pole-ward of 20°, with amplitudes continuing to grow at higher latitudes. The amplitudes in the Southern (SH) and Northern Hemisphere (NH) reach peaks at approximately the same altitudes: one in the upper stratosphere (45 km) and the other in the mesopause (85 km).

177   A comparison between the peaks observed in the two Hemispheres reveals an obvious
178   asymmetry. In the mesopause, the AO amplitudes are larger in the NH than in the SH, with the
179   situation being reversed in the stratosphere. In addition, the oscillations are stronger in the upper
180   mesosphere than in the upper stratosphere, with a local minimum at 65 km. This result is in
181   agreement with that of Dou et al. [1]. The global pattern of the AO is similar to that reported by Xu et
182   al. [10]. However, there are differences above 70 km, where the amplitude peaks derived by these
183   authors are larger than those in this work. This could be due in part to the extraction methods and
184   the time period of the data, but even more importantly because of the data version (SABER
185   temperature data of versions 1.06 and 2.0). As discussed above, there have been substantial
186   improvements in the non-LTE algorithm above 70 km in versions after 1.06.

187   As shown in Figure 2b, temperature AOs in the stratosphere and the mesosphere are mostly out
188   of phase between the two Hemispheres. Note that the phase terms in (1) represent the times at which
189   temperatures are highest. Because of the shifting of the direct sunlight, it is easy to understand that
190   both of the NH and the SH have higher temperature in summer than in winter at the stratosphere
191   (from ~30–60 km). But this situation completely changes in mesosphere (from ~80–95 km), that the
192   peak NH and SH phases are around the winter and summer solstices, respectively. Mayr et al. [24]
193   account for this reversal when considered the GW filtering.

194   The temporal variations of zonal mean temperatures in Figure 3 support the analysis of
195   amplitude asymmetry and phase reversal between the two Hemispheres. Apart from that, it is
196   salient that the SH summer is warmer than the NH one at both 45 and 85 km. This agrees with Xu et
197   al. [25], whose results show that warmer temperatures occur in the SH summer than in the NH one,
198   from 20 km up to the mesopause. The causes of this phenomenon include gravity-wave filtering and
199   the solar flux variation arising from the Earth's orbital eccentricity [26-27].

200   The wavelet power spectrum results, used to determine the dominant variations and how they
201   vary with time, are presented in Figure 4. The thick-contour-enclosed regions in the wavelet power
202   spectrum and the AO peaks well above the dashed line in the global wavelet power spectrum
203   indicate that AO dominates the mid-latitudes at 45 and 85 km. In addition, the blank regions at the
204   top of each wavelet power spectrum suggest that the smaller periodicities are well separated from
205   the mean variations by our method.

206   Figure 5 gives the variations of AO phase and amplitude. At 45 km, the amplitudes at 50°N and
207   50°S share the same tendency except for 2005 and 2014, and a 3-year periodicity is seen in 50°S. At 85
208   km, there is a 6-year periodicity at 50°S, while the variation at 50°N exhibits a 2-year period between
209   2005 and 2011. As shown in Figure 5b, all the AO phases show weak inter-annual variations.

(**a**)   (**b**)
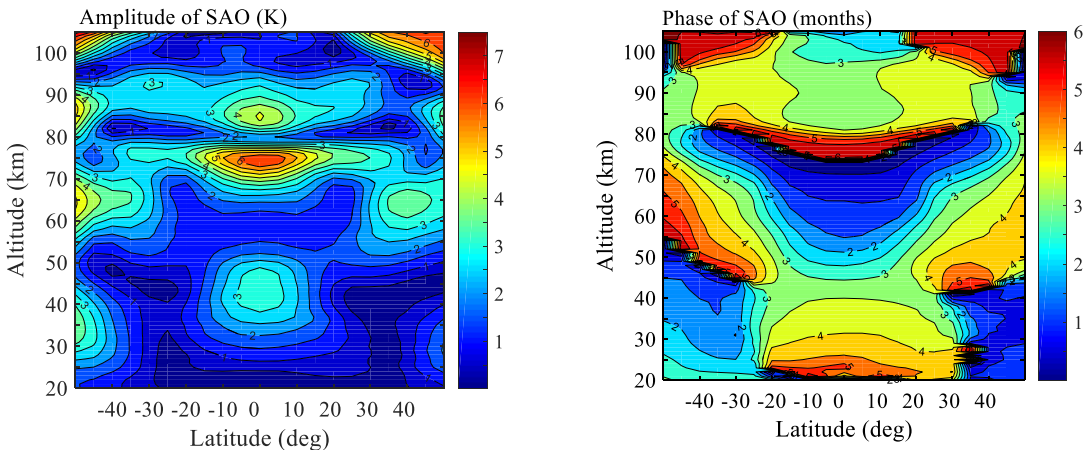
210   Figure 6. Distribution of (a) the amplitude (K) and (b) phase (months) of SAO.

211   Contour intervals are 0.5 K and 0.5 month.

212

(**a**)

(b)

(c)
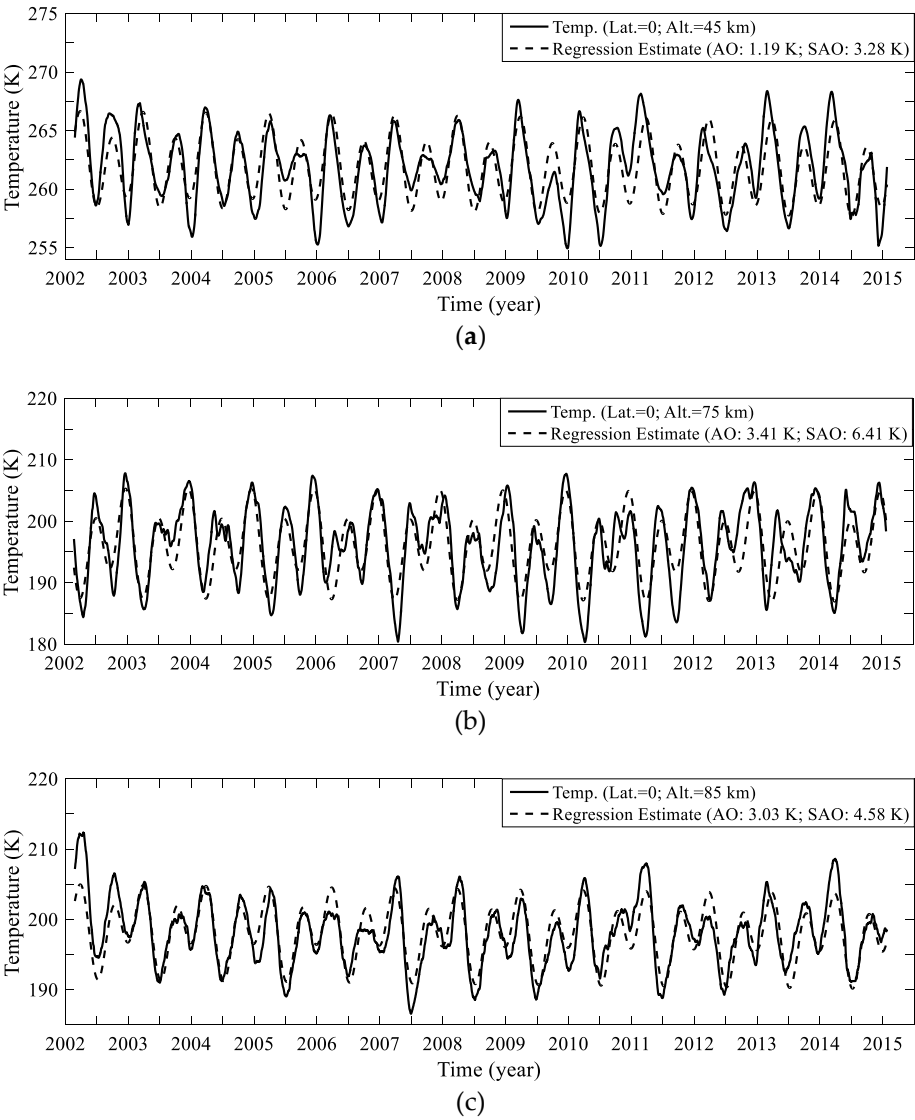
213   Figure 7. Time series of zonal mean temperature at the equator.

214   (a) for 45 km, (b) for 75 km, (c) for 85 km.

215

(**a**)   (b)

(c)   (d)

(e)   (f)
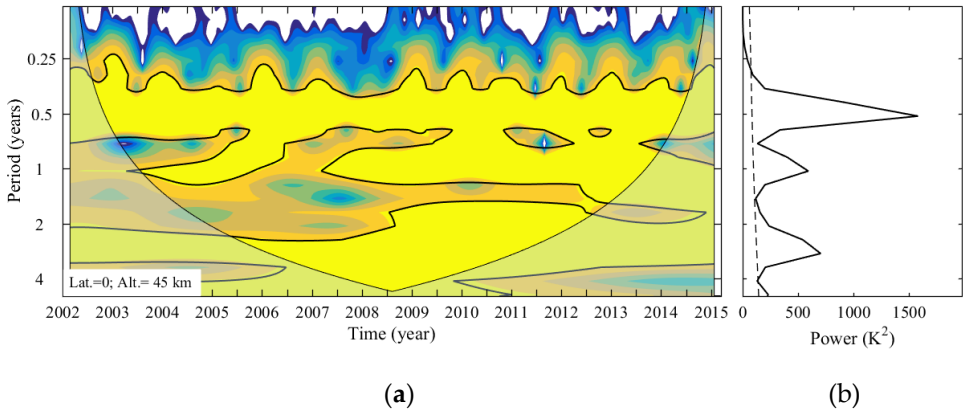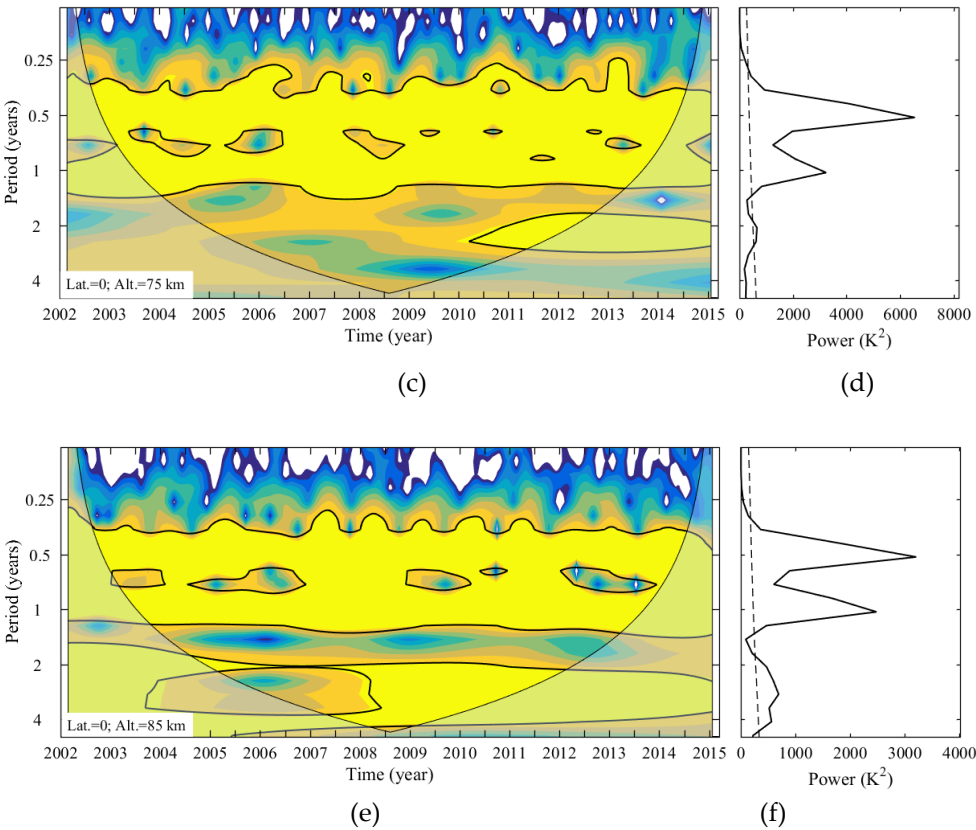
Figure 8. The wavelet power spectrum and the global wavelet spectrum at the equator.
(a) (b) for 45 km, (c) (d) for 75 km and (e) (f) for 85 km.

(**a**)   (**b**)
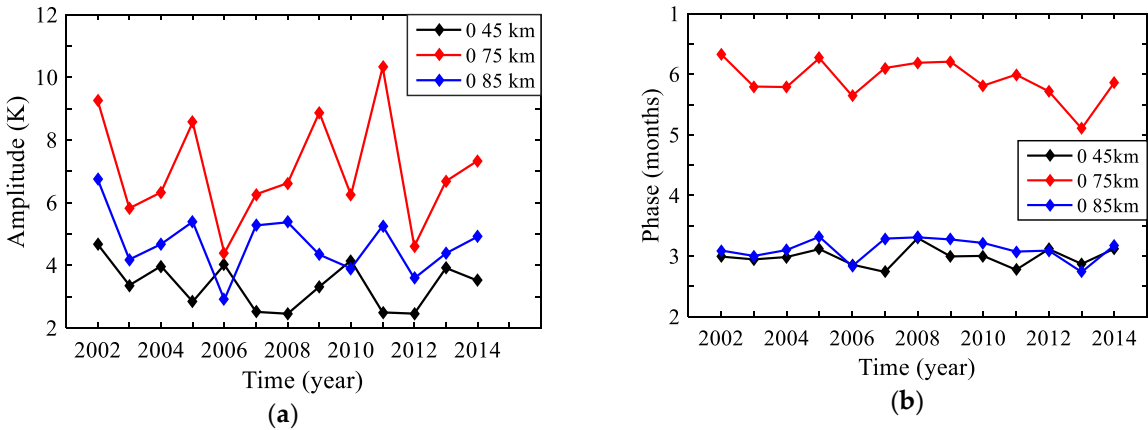
Figure 9. Variations of (a) the amplitudes and (b) phases of the SAO at the equator at 45, 75,
and 85 km.

4.2. Semiannual oscillation (SAO)

The SAO was first identified by Reed [28] in stratospheric tropical temperature measurements
by radiosonde. A mesospheric SAO has also been identified and analyzed (e.g. [29-30]). The research
of Baumgaertner [31] demonstrates that gravity waves are universal in the middle atmosphere and
play an important role in middle-atmospheric dynamics. It is believed that gravity waves and the
momentum advection are the main causes of the tropical SAO [24,32].

228   Presented in Figure 6 are the amplitude and phase of the SAO based on SABER temperatures
229   from 2002 to 2015 at altitudes of 20–105 km and latitudes from 50°S to 50°N. It is found that the
230   global distributions of the SAO amplitude and phase are almost symmetrical with respect to the
231   equator, and that the SAO amplitude tends to be strongest within 20° of the equator. In the tropical
232   regions, the stratospheric SAO has a peak of >3 K in the 40–50-km layer. The mesospheric SAO has
233   two amplitude maxima: one >6 K at 75 km, and the other ~4.5 K at 85 km. After diminishing between
234   20°–40°, the amplitude increases again at latitudes pole-ward of 40°. Its magnitude, however, is
235   smaller than that of the AO at mid-latitudes, which means that the SAO is weaker there. In addition,
236   comparing the phases of AO and SAO in Figure 2b and 6b, we find that the SAO's phases appear
237   obviously vertical gradients, especially around the regions where SAOs maximize. However, it is
238   not the case of AO. This may mean that the SAO is a kind of propagation mode. .

239   The time series of SABER temperatures from January 2002 to February 2015 at the altitudes
240   where the SAO is strongest are presented in Figure 7. In the tropical regions, the phases of the SAO
241   in the upper stratosphere (45–50 km) are around the equinox and are mostly in phase with those in
242   the UMLT. In the mesosphere below 80 km, the phase propagates downward rapidly at altitudes of
243   80–75 km. The temporal variation at 75 km shown in Figure 7b is consistent with the results of
244   Shepherd et al. [33]. The SAO reaches its minima at the spring and autumn equinoxes, whereas it
245   peaks at the summer and winter solstices. The SAO at 75 km is mainly out of phase with that at 85
246   km. The phase reversal that takes place at ~82 km is linked to the lower mesospheric inversion layers,
247   as will be discussed in detail in section 5.

248   We now consider the wavelet spectrum of the SAO at the equator. Figure 8 shows that SAO is
249   the dominant oscillation at the equator, although AO peaks are also present at this latitude. In
250   addition, comparing with Figure 1, the ternary component can be seen to have been a salient
251   oscillation at 45 and 85 km throughout most of 2002–2015.

252   In parallel with the AO, the variations of SAO amplitudes and phases from 2002 to 2014 are
253   shown in Figure 9. Figure 9a shows that the amplitude presents prominent inter-annual variations at
254   both 75 and 85 km. These have similar trends, with maximum amplitudes in 2002, 2005, and 2011;
255   both exhibit a period of ~3 years. However, the inter-annual amplitude variation is weaker at 45 km,
256   and its periodicity is not significant. The analysis of SAO phase is similar to that of AO, which
257   showed relatively weak inter-annual variation.

258
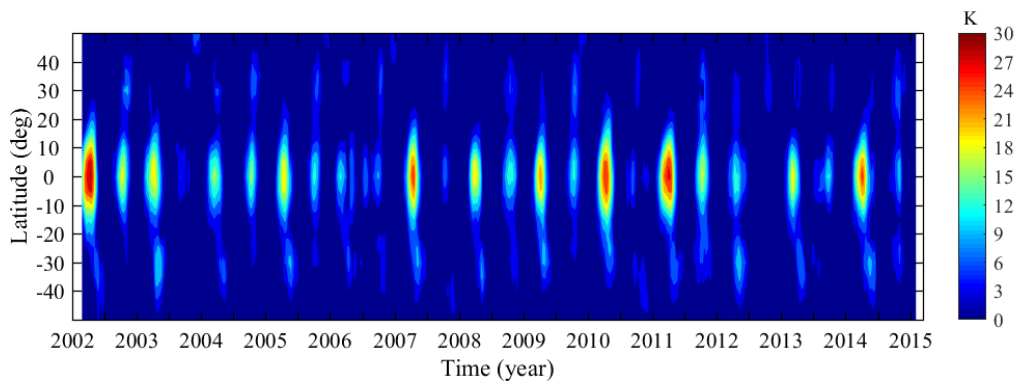
259   Figure 10. Zonal mean temperature amplitudes of the lower MIL, 2002–2015.
260   Contour interval is 3 K.
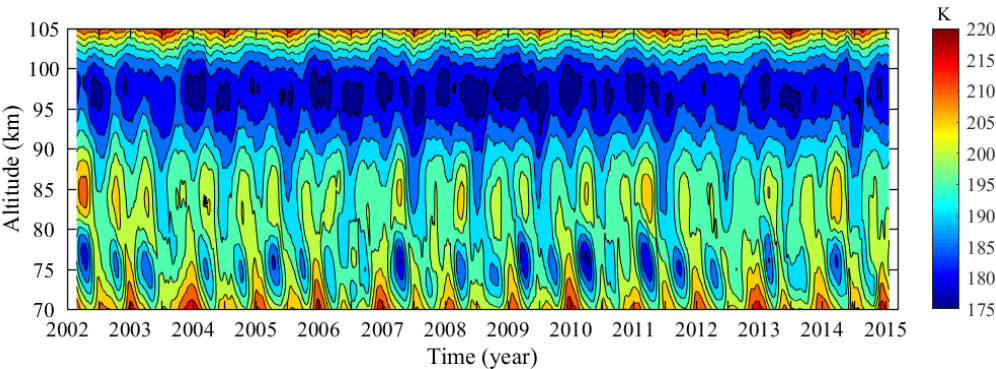
261   Figure 11. Variation of zonal mean temperature at the equator.
262   Contour interval is 5 K.
263
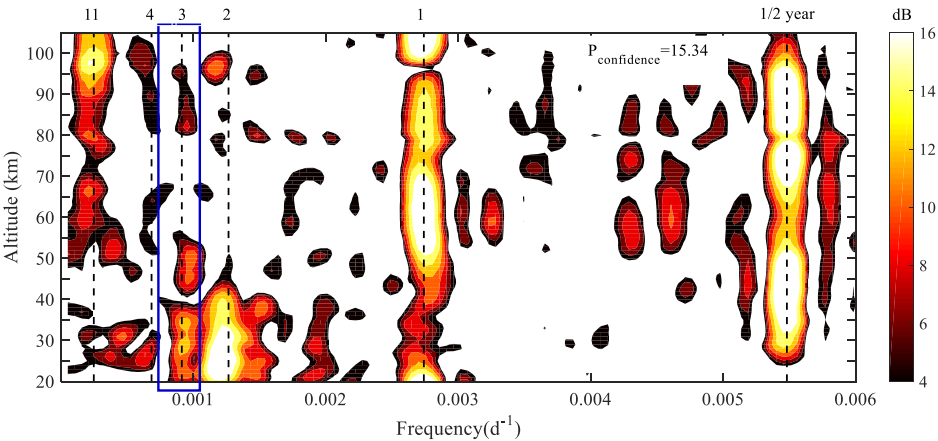
264   Figure 12. Lomb–Scargle spectral analysis of zonal mean temperature at the equator.
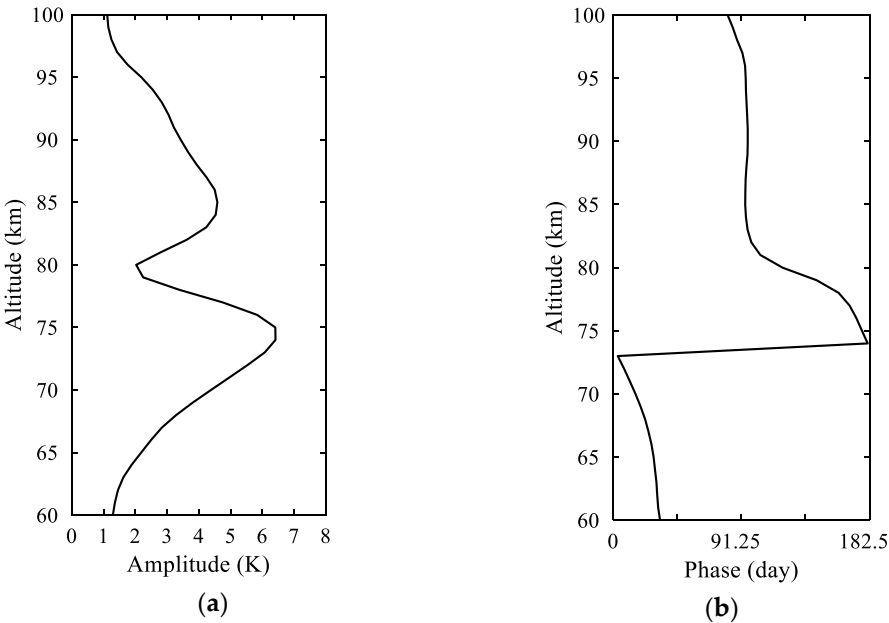
265   Figure 13. Vertical structure of (a) amplitude and (b) phase of the SAO at the equator.
266

5. The lower mesospheric inversion layer

The term 'mesospheric inversion layer' (MIL) is defined from the fact that the lapse rate of the temperature is positive at specific layers in the mesosphere. Studies have revealed that the MIL can be divided into two sub-layers: the lower and the upper MILs at approximately 75 and 90 km, respectively (e.g. [5,34]). The following discussion is concerned with the lower MIL.

In order to extract the lower MILs from the background temperature, we use the method analogous to Gan et al. [35], whereby 3-day averaged vertical temperature profiles are used to identify the local maximum and minimum nodes at 65–85 km. The largest difference between successive such nodes is then identified as the amplitude of the lower MIL. Note that the 60-day average temperature data are used here, rather than 3-day ones. As mentioned in section 2, using data in this manner can smooth out the tidal and planetary-wave perturbations. However, the prominent tidal aliasing in the equatorial mesosphere may still affect the results.

The temporal variation of the lower MIL amplitude is shown in Figure 10. The largest amplitudes of the lower MIL occur in regions within 15° of the equator. The amplitude peaks are largest during almost every equinox, and contain evident semi-annual cycles. Note that the peaks at the spring equinox appear to be more robust than those at the autumn one.

Figure 11 presents the variation of background zonal mean temperature at the equator. The temperature increases during each spring and autumn equinox between 75 and 85 km. This increase is synchronous with the existence of MIL amplitude maxima, indicating that the structure of the mesospheric SAO may cause the tropical lower MIL.

The contribution of SAO to the MIL is analyzed quantitatively in this section. The Lomb–Scargle spectral analysis of time-versus-altitude data is shown in Figure 12, where it can be seen that SAO is the strongest oscillation at both 75 and 85 km. These altitudes correspond to the bottom (75 km) and top (85 km) of the lower MIL. Figure 13 shows that the amplitude reaches peaks at 75 and 85 km, and the respective phases are around both solstices and both equinoxes. The SAO phase changes rapidly from 75 to 85 km. This feature may cause the temperature increase between 75 and 85 km at each equinox, resulting in a temperature inversion of ~11 K at the equator. This result is similar to that of Gan et al. (35), although they found that the SAO contribution to the lower MIL was ~12 K.

The question arises as to why the MIL amplitude is more robust during the spring equinox than during the autumn one, as shown in Figure 10. Tidal aliasing at the mesosphere may account for this observation. The amplitudes of diurnal tides are generally larger around an equinox, when we expect the background temperature to be affected more [16] and the diurnal migrating tides at the mesosphere to contribute to the lower MIL at the equator by 20–30 K [35].

(**a**)   (**b**)
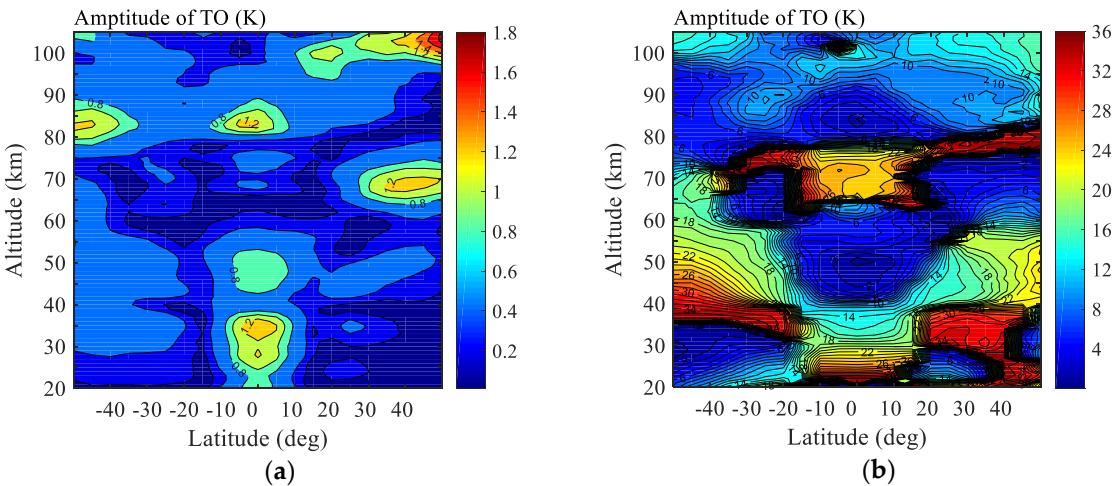
Figure 14.   Distribution of (a) the amplitude (K) and (b) phase (months) of TO.
Contour intervals are 0.2 K and 4 month.
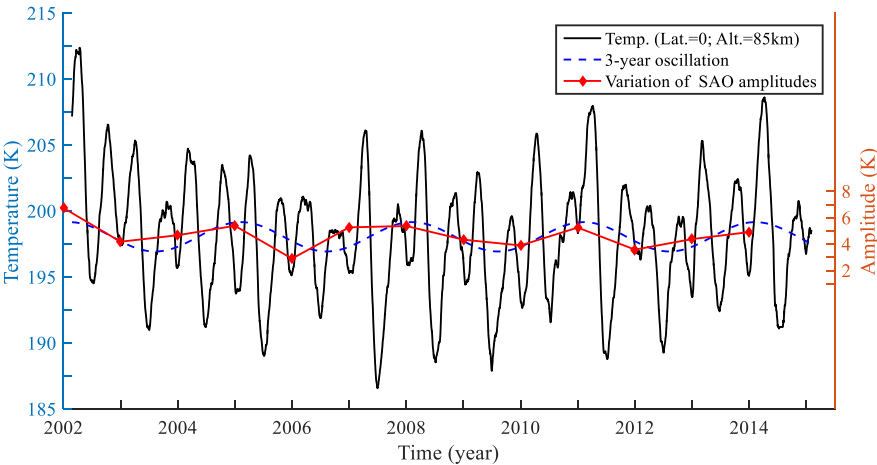
Figure 15. Variations of the TO and the SAO amplitudes at 85km at the equator.
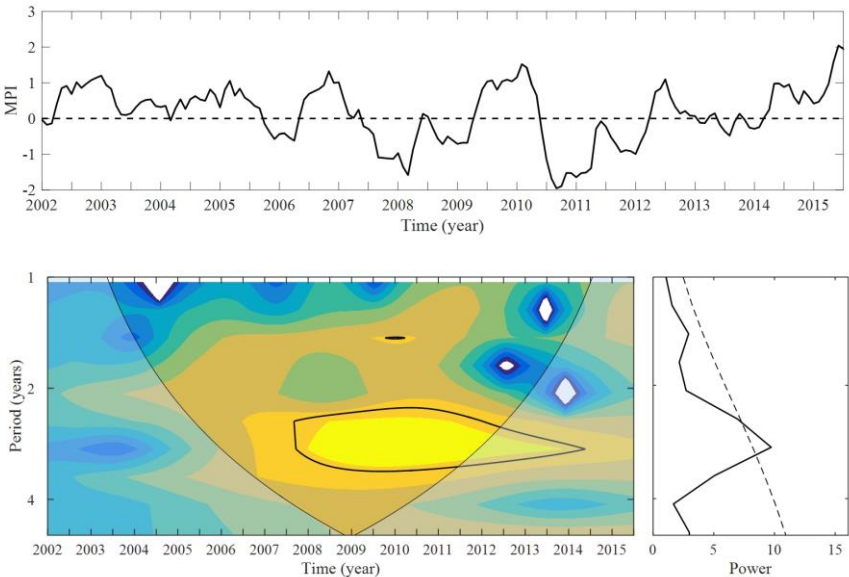
305   Figure 16. Variation of the MEI and the corresponding wavelet power spectrum and global

306   wavelet spectrum. (The Multivariate ENSO Index is dimensionless)

307

308

6. The triennial oscillation (TO)

310   As seen in both the lomb-scargle (Figure 1) and wavelet spectra (Figure 8), the TO is prominent
311   in the mesosphere, especially in the tropical region. As illustrated in the blue-line box of Figure 12,
312   the strong signal of TO can be seen in most of the stratosphere and ~85 km in the mesosphere at the
313   equator. The amplitude and phase of TO as a function of altitude and latitude are extracted in the
314   residual error in equation (1), using the nonlinear least squares fitting method.

315   The global structures of amplitude and phase of TO are shown in Figure 14. The amplitude of
316   the TO is no more than 2 K. This is much smaller than that of the AO and SAO. Hence, the TO signal
317   is generally obscured by the AO in the mid-latitudes, where the AO amplitude can approach >10 K.
318   In the tropical region, the TO has three amplitude maxima : two in the stratosphere (35 km and 45
319   km) and one in the mesosphere (85 km). The amplitudes are ~1.2 K, ~0.8 K and ~1.2 K respectively.
320   The phases at 45 km and 85 km are ~2th month, while the phase at 35 km is ~14th month.

321   As mentioned in section 4, 3-year periodicities in the AO and SAO are seen at 45 km and 50 S,
322   as well as 75-85 km over the equator in Figures 5 and 9. Is it related to the TO detected in the
323   background temperature? Figure 15 shows the interannual variation of amplitudes of SAO and the
324   variation of TO at 85 km at the equator. It seems that the two time series are in phase and share the
325   similar amplitudes. However, the 3-year periodicities in the SAO and AO at 75 km over the equator
326   and at 45km and 50 S ,respectively, are out of phase with the TO in the same altitudes and latitudes
327   (figures not shown). It suggests that there may be potential interaction by the TO with SAO mainly
328   at ~85 km at the equator.

329   The origins of the TO in the zonal mean temperature remain a problem. Several studies has
330   revealed that the tropical stratospheric temperature changes are influenced by several forces
331   including: (1) the solar activities, (2) the quasi-biennial oscillation in the zonal winds, (3) the volcanic
332   activities, (4) the El Niño–Southern Oscillation (ENSO) [36-38].The ENSO variations can be
333   characterized by the Multivariate ENSO Index (MEI) [39]. As seen in Figure 16, the MEI has a
334   significant 3-year oscillation from year 2008 to 2014. So, whether or not ENSO is the origin of the TO
335   in the middle atmosphere? The ENSO signals can influence the middle atmosphere by means of
336   planetary wave. In the tropical region, the rhythmic warming and cooling signal of ENSO are
337   usually accompanied by the opposite sign in the lower stratospheric zonal mean temperature [37].
338   However, this ENSO-related influence is not discernible above ~23 km at the equator [36, 40], where
339   the TO is significant. Above all, we believe that the ENSO signal may modulate the amplitude of the
340   TO, mainly in the lower stratosphere. The real origin of the TO may possiblely lie in the
341   wave-mean-flow interaction, which need our further research.

342

7. Conclusions

344   Based on SABER 2.0 temperature data from January 2002 to February 2015, we have used a
345   60-day sliding window to derive the zonal mean temperature. Lomb–Scargle and wavelet spectral
346   were used in this paper to determine the significant oscillations in the background temperature field.

347   By applying the nonlinear least-squares fitting method, the global structure of AO ,SAO and TO
348   were investigated, along with their inter-annual variations.

349   The AO is the dominant oscillation at mid-latitudes in both the stratosphere and mesosphere,
350   with amplitudes increasing pole-ward. The AO amplitudes present an obvious asymmetry between
351   the two Hemispheres. In the mesosphere, the AO amplitudes are larger in the NH than in the SH,
352   with the situation being reversed in the stratosphere. In addition, the oscillations are stronger in the
353   mesosphere than in the stratosphere. At mid-latitudes, the stratospheric and mesospheric
354   temperature AOs in the SH are mostly out of phase with those in the NH. The AO amplitudes
355   contain evident inter-annual variations, with changing periodicity at different altitudes, but the AO
356   phases present only relatively weak inter-annual variations.

357   The SABER zonal mean temperature shows a prominent SAO in the tropical areas with three
358   amplitude maxima: one in the stratosphere (45 km) and two in the mesosphere (75 and 85 km). The
359   amplitude maxima at 75 km are the largest among the three, reaching a peak of ~7 K. The SAOs at 45
360   km are in phase with those at 85 km, but are out of phase with those at 75 km. A phase inversion can
361   be identified between 75 and 85 km. The amplitudes at both 75 and 85 km contain prominent
362   inter-annual variations that have similar trends, each exhibiting a period of ~3 years.

363   The SAO is closely associated with the lower MIL. The largest amplitudes of the lower MIL fall
364   in the regions within 15° of the equator. The amplitude peaks are largest during almost every
365   equinox, showing prominent semi-annual cycles. Note that the phase inversion that occurs at ~82 km
366   may be the cause of the 11-K enhancement in the background temperature. However, our results are
367   contaminated to a certain extent by tidal aliasing, especially by the diurnal tide that has some
368   features in common with the zonal mean SAO. Thus, a temperature data set of comprehensive local
369   time coverage is needed to reduce tidal aliasing in the equatorial upper mesosphere.

370   The TO is significant in the tropical region, having relative smaller amplitude compared with
371   that of AO and SAO. There are three amplitude maxima of the TO at the equator: two in the
372   stratosphere (35 km and 45 km) and one in the mesosphere (85 km). The 3-year periodicities in the
373   SAO match well with the TO at 85km at equator, indicating the potential interaction by the TO with
374   SAO there. The relation between ENSO and TO has also been discussed. Results are that the ENSO
375   signal may modulate the amplitude of the TO, mainly in the lower stratosphere, and the real origin
376   of the TO may possibly lie in the wave-mean-flow interaction, which need our further research.

377

378   **Acknowledgments:** The SABER data used here were provided by the TIMED/SABER team, and we would like
379   to acknowledge their contributions to this work. The study was partly supported by the National Nature
380   Science Foundation of China (Grant no. 41375028), and the National Nature Science Foundation of Jiangsu,
381   China (Grant no. BK20151446)

382   **Author Contributions:** Shudao Zhou, Hanqing Shi and Zheng Sheng conceived and designed the experiments;
383   Yiyao Zhang ,Zhiqiang Fan and Huadong Du performed the experiments; Yiyao Zhang and Weilai Shi
384   analyzed the data; Yiyao Zhang wrote the paper.

385

386

References

1.   Dou, X.; Li, T.; Xu, J.; Liu, H. L.; Xue, X.; Wang, S.; Leblanc, T.; Mcdermid, I. S.; Hauchecorne, A.; Keckhut, P. Seasonal oscillations of middle atmosphere temperature observed by Rayleigh lidars and their comparisons with TIMED/SABER observations. *J. Geophys. Res.* **2009**, *114*, 311-311.

2.   Hocking, W. K. Temperatures Using radar-meteor decay times. *Geophys. Res. Lett.* **1999**, *26*, 3297–3300.

3.   Sheng, Z.; Jiang, Y.; Wan, L.; Fan, Z. Q. A Study of Atmospheric Temperature and Wind Profiles Obtained from Rocketsondes in the Chinese Midlatitude Region. *J. Atmos. Ocean. Technol.* **2015**, *32*,722–735.

4.   Wang, Z.; Chang, C. P.; Wang, B.; Jin, F. F. Teleconnections from tropics to northern extratropics through a southerly conveyor . *J. Atmos. Sci.* **2005**, *62*, 4057-4070.

5.   Clancy, R. T.; Rusch, D. W.; Callan, M. T. Temperature minima in the average thermal structure of the middle mesosphere (70–80 km) from analysis of 40- to 92-km SME global temperature profiles. *J. Geophys. Res.* **1994**, *99*, 19001–19020.

6.   Leblanc, T.; Hauchecorne, A. Recent observations of mesospheric temperature inversions. *J. Geophys. Res.* **1997**, *102*, 19471–19482.

7.   Remsberg, E. E.; Bhatt, P. P.; Deaver, L. E. Seasonal and longer-term variations in middle atmosphere temperature from HALOE on UARS. *J. Geophys. Res.* **2002**, *107*, ACL 18-1–ACL 18-13.

8.   Anthes, R. A.; Bernhardt, P. A.; Chen, Y.; Cucurull, L.; Dymond, K. F.; Ector, D.; Healy, S. B.; Ho, S. P.; Hunt, D. C.; Kuo, Y. H. The COSMIC/FORMOSAT-3 Mission: Early Results. *Bull. Amer. Meteor. Soc.* **2008**, *89*, 313-333.

9.   Huang, F. T.; Mayr, H. G.; Reber, C. A.; Russell, J. M.; Mlynczak, M.; Mengel, J. G. Stratospheric and mesospheric temperature variations for the quasi-biennial and semiannual (QBO and SAO) oscillations based on measurements from SABER (TIMED) and MLS (UARS). *AnGeo* **2006**, *24*, 2131-2149.

10. Xu, J.; Smith, A. K.; Yuan, W.; Liu, H. L.; Qian, W.; Mlynczak, M. G.; Russell, J. M. Global structure and long-term variations of zonal mean temperature observed by TIMED/SABER. *J. Geophys. Res.* **2007**, *112*, 177-180.

11. Mertens, C. J.; Mlynczak, M. G.; Manuel, L. P.; Wintersteiner, P. P.; Picard, R. H.; Winick, J. R.; Gordley, L. L.; Russell, J. M. Retrieval of Mesospheric and Lower Thermospheric Kinetic Temperature from Measurements of CO_2 15 Micrometers Earth Limb Emission under Non-LTE Conditions. *Geophys. Res. Lett.* **2001**, *28*, 1391-1394.

12. Mertens, C. J.; Schmidlin, F. J.; Goldberg, R. A.; Remsberg, E. E.; Dean, P. W.; Russell, J. M.; Mlynczak, M. G.; Manuel, L. P.; Wintersteiner, P. P.; Picard, R. H. SABER observations of mesospheric temperatures and comparisons with falling sphere measurements taken during the 2002 summer MaCWAVE campaign. *Geophys. Res. Lett.* **2004**, *31*, 445-446.

13. Fan, Z. Q.; Sheng, Z.; Shi, H. Q.; Yi, X.; Jiang, Y.; Zhu, E. Z. Comparative Assessment of COSMIC Radio Occultation Data and TIMED/SABER Satellite Data over China. *J. Climate. Appl. Meteor.* **2015**, *54*, 1931-1943.

14. Remsberg, E. E.; Marshall, B. T.; Garcia-Comas, M.; Krueger, D.; Lingenfelser, G. S.; Martin-Torres, J.; Mlynczak, M. G.; Iii, J. M. R.; Smith, A. K.; Zhao, Y. Assessment of the quality of the Version 1.07 temperature-versus-pressure profiles of the middle atmosphere from TIMED/SABER. *J. Geophys. Res.* **2008**, *113*, 1641-1653.

15. Mcdonald, A. J.; Baumgaertner, A. J. G.; Fraser, G. J.; George, S. E.; Marsh, S. Empirical Mode Decomposition of the atmospheric wave field. *AnGeo* **2007**, *25*, 255-270.

16. Oberheide, J.;Hagan, M. E.;Roble, R. G. Tidal signatures and aliasing in temperature data from slowly precessing satellites. *J. Geophys. Res.* **2003**, *108*, 565-565

17. Zhu, X.; Yee, J. H.; Talaat, E. R.; Mlynczak, M.; Gordley, L.; Mertens, C.; Russell, J. M. An algorithm for extracting zonal mean and migrating tidal fields in the middle atmosphere from satellite measurements: Applications to TIMED/SABER–measured temperature and tidal modeling. *J. Geophys. Res.* **2005**, *110*, 57–66.

18. Press, W. H.; Teukolsky S. A.; Vetterling W. T. et al. **1992**: Numerical Recipes in FORTRAN, 2nd ed.   New York: Cambridge University Press, 569–577.

19. Torrence, C.; Compo, G. P. A Practical Guide to Wavelet Analysis. *Bull. Amer. Meteor. Soc.* **1998**, *79*, 61-78

20. Huang, F. T.; Mayr, H. G.; Reber, C. A.; Iii, J. M. R.; Mlynczak, M. G.; Mengel, J. G. Ozone quasi-biennial oscillations (QBO), semiannual oscillations (SAO), and correlations with temperature in the mesosphere, lower thermosphere, and stratosphere, based on measurements from SABER on TIMED and MLS on UARS. *J. Geophys. Res.* **2008**, *113*, 405-418.

21. Clemesha, B.; Takahashi, H.; Simonich, D.; Gobbi, D.; Batista, P. Experimental evidence for solar cycle and long-term change in the low-latitude MLT region. *J. Atmos. Terr. Phys.* **2005**, *67*, 191-196.

22. Huang, F. T.; Mayr, H. G.; Russell, J. M., Iii; Mlynczak, M. G. Ozone and temperature decadal responses to solar variability in the mesosphere and lower thermosphere, based on measurements from SABER on TIMED. *AnGeo* **2016**, *34*, 29-40.

23. Kane, R. P.; Buriti, R. A. Latitude and Altitude Dependence of the Interannual Variability and Trends of Atmospheric Temperatures. *Pure. Appl. Geophys.* **1997**, *149*, 775-792.

24. Mayr, H.;Mengel, J.;Chan, K.;Huang, F. Middle atmosphere dynamics with gravity wave interactions in the numerical spectral model: Zonal-mean variations. *J. Atmos. Terr. Phys* **2010**, *72*, 807-828.

25. Xu, J.; Liu, H. L.; Yuan, W.; Smith, A. K.; Roble, R. G.; Mertens, C. J.; Iii, J. M. R.; Mlynczak, M. G. Mesopause structure from Thermosphere, Ionosphere, Mesosphere, Energetics, and Dynamics (TIMED)/Sounding of the Atmosphere Using Broadband Emission Radiometry (SABER) observations. *J. Geophys. Res.* **2007**, *112*, 139-155.

26. Chu, X.;Gardner, C. S.;Roble, R. G. Lidar studies of interannual, seasonal, and diurnal variations of polar mesospheric clouds at the South Pole. *J. Geophys. Res.* **2003**, *108*, 347-362

27. Siskind, D. E.;Eckermann, S. D.;Mccormack, J. P.;Alexander, M. J.;Bacmeister, J. T. Hemispheric differences in the temperature of the summertime stratosphere and mesosphere. *J. Geophys. Res.* **2003**, *108*, -.

28. Reed, R.J. Some features of the annual temperature regime in the tropical stratosphere, *Mon. Weath. Rev* **1962**, *90*, 211–215.

29. Angell, J. K.;Korshover, J. Quasi-Biennial, Annual, and Semiannual Zonal Wind and Temperature Harmonic Amplitudes and Phases in the Stratosphere and Low Mesosphere of the Northern Hemisphere. *J. Geophys. Res.* **1970**, *75*, 543-550.

30. Garcia, R. R.; Dunkerton, T. J.; Lieberman, R. S.; Vincent, R. A. Climatology of the semiannual oscillation, of the tropical middle atmosphere, *J. Geophys. Res.* **1997**, *102*, 26019-26032.

31. Baumgaertner, A. J. G. Observations of Middle Atmosphere Dynamics over Antarctica. Doctoral dissertation, University of Canterbury, Christchurch, New Zealand, **2007**.

32. Hamilton, K. Dynamics of the stratospheric semiannual oscillation. *J. Meteor. Soc. Japan.* **1986**, *64*, 227–244.

33. Shepherd, M. G.; Evans, W. F. J.; Hernez, G.;Dirk, O.; Hisao, T. Global variability of mesospheric temperature: Mean temperature field. *J. Geophys. Res.* **2004**, *109*, 89-92.

34. Meriwether, J. W.; Gardner, C. S. A review of the mesosphere inversion layer phenomenon. *J. Geophys. Res.* **2000**, *105*, 12405-12416.

35. Gan, Q.; Zhang, S. D.; Yi, F. TIMED/SABER observations of lower mesospheric inversion layers at low and middle latitudes. *J. Geophys. Res.* **2012**, *117*, 134-142.

36. Reid, G. C. Seasonal and interannual temperature variations in the tropical stratosphere. *J. Geophys. Res.* **1994**, *99*, 18923-18932.

37. Randel, W. J.; Garcia, R. R.; Calvo, N.; Dan, M. ENSO influence on zonal mean temperature and ozone in the tropical lower stratosphere. *Geophys. Res. Lett.* **2009**, *36*, 172-173.

38. Seidel, D. J.; Li, J.; Mears, C.; Moradi, I.; Nash, J.; Randel, W. J.; Saunders, R.; Thompson, D. W. J.; Zou, C. Z. Stratospheric temperature changes during the satellite era. *J. Geophys. Res.* **2016**, *121*,664-681.

39. Wolter, K.; Timlin, M. S. El Niño/Southern Oscillation behaviour since 1871 as diagnosed in an extended multivariate ENSO index (MEI.ext). *Int J Climatol.* **2011**, *31*, 1074–1087.

40. García-Herrera, R.; Calvo, N.; Garcia, R. R.; Giorgetta, M. A. Propagation of ENSO temperature signals into the middle atmosphere: A comparison of two general circulation models and ERA-40 reanalysis data. *J. Geophys. Res.* **2006**, *111*, 831-846.